Evaluation of SF_6, C_2Cl_4, and CO to approximate fossil fuel CO_2 in the Northern Hemisphere using a chemistry transport model

Leonard Rivier, Philippe Ciais, Didier Hauglustaine, Peter Bakwin, Philippe Bousquet, Philippe Peylin, A. Klonecki

Evaluation of SF_6, C_2Cl_4, and CO to approximate fossil fuel CO_2 in the Northern Hemisphere using a chemistry transport model

L. Rivier,[1] P. Ciais,[1] D. A. Hauglustaine,[1] P. Bakwin,[2] P. Bousquet,[1] P. Peylin,[1] and A. Klonecki[1,3]

Received 30 September 2005; revised 3 April 2006; accepted 23 May 2006; published 25 August 2006.

[1] The distribution of the fossil fuel component in atmospheric CO_2 cannot be measured directly at a cheap cost. Could anthropogenic tracers with source patterns similar to fossil fuel CO_2 then be used for that purpose? Here we present and evaluate a methodology using surrogate tracers, CO, SF_6, and C_2Cl_4, to deduce fossil fuel CO_2. A three-dimensional atmospheric chemistry transport model is used to simulate the relationship between each tracer and fossil fuel CO_2. In summertime the regression slopes between fossil fuel CO_2 and surrogate tracers show large spatial variations for chemically active tracers (CO and C_2Cl_4), although C_2Cl_4 presents less scatter than CO. At two tall tower sites in the United States (WLEF, Wisconsin, and WITN, North Carolina), we found that in summertime the C_2Cl_4 (CO) versus fossil CO_2 slope is on average up to 15% (25%) higher than in winter. We show that for C_2Cl_4 this seasonal variation is due to OH oxidation. For CO the seasonal variation is due to both chemistry and mixing with nonanthropogenic CO sources. In wintertime the three surrogate tracers SF_6, C_2Cl_4, and CO are about equally as good indicators of the presence of fossil CO_2. However, our model strongly underestimates the variability of SF_6 at both towers, probably because of unaccounted for emissions. Hence poor knowledge of emission distribution hampers the use of SF_6 as a surrogate tracer. From a practical point of view we recommend the use of C_2Cl_4 as a proxy of fossil CO_2. We also recommend the use of tracers to separate fossil CO_2. Despite the fact that the uncertainty on the regression slope is on the order of 30%, the tracer approach is likely to have less bias than when letting one model with one inventory emission map calculate the fossil CO_2 distribution.

Citation: Rivier, L., P. Ciais, D. A. Hauglustaine, P. Bakwin, P. Bousquet, P. Peylin, and A. Klonecki (2006), Evaluation of SF_6, C_2Cl_4, and CO to approximate fossil fuel CO_2 in the Northern Hemisphere using a chemistry transport model, *J. Geophys. Res.*, *111*, D16311, doi:10.1029/2005JD006725.

1. Introduction

[2] This paper investigates the role of ancillary tracers in helping to determine the fossil fuel component of atmospheric CO_2. Fossil fuel emissions are the largest term of the human induced perturbation of the global carbon cycle, and they drive the long-term increase of atmospheric CO_2. Annual totals of fossil fuel emissions for the globe have errors estimated to be 6–10% [*Marland and Rotty*, 1984]. The average national emission total has perhaps a 8% uncertainty associated with it. However, uncertainties may range from −340% to 90% for a given country and year [*Andres et al.*, 1999]. Also, the space and time pattern of fossil fuel emissions, is more uncertain than the emission country totals. Generally, human population density, for example, is used to distribute the country totals, ignoring or simplifying patterns of energy use and energy production, such as electricity generation from fuel burning, habitat heating and cooking, and transportation. When applying atmospheric inversions to CO_2 concentrations measurements, fossil fuel fluxes are rarely sought in their own right. They are rather constrained separately from terrestrial or oceanic sources or sinks. The most common approach consists in calculating, with a transport model, the atmospheric CO_2 gradients due to fossil fuel emissions, and then subtracting this signal from station observations to invert the residual natural fluxes over different regions. Doing so propagates two kinds of systematic errors in the inversions. First, using a fixed a priori pattern of fossil fuel emissions might generate errors in ascribing fluxes to the biosphere and the oceans rather than to the fixed fossil fuel emissions. Second, transport models have biases in simulating the time varying distribution of fossil fuel CO_2 ($FFCO_2$) in the atmosphere. Those biases are unknown because there is (almost) no direct measurement of $FFCO_2$, but a lower limit of those biases can be recognized by taking the spread

[1] Laboratoire des Sciences du Climat et de l'Environnement, CEA, Gif sur Yvette, France.
[2] Climate Monitoring and Diagnostics Laboratory, National Oceanic and Atmospheric Administration, Boulder, Colorado, USA.
[3] Now at NOVELTIS, Parc Technologique du Canal, Ramonville-Saint Agne, France.

0148-0227/06/2005JD006725

between different transport model results. *Gurney et al.* [2004] found for instance that transport model differences are on the order of 20% in simulating fossil CO_2 response functions at two tall towers in the United States.

[3] In order to quantify the fossil fuel component of the CO_2 concentration, it is tantalizing to use measurements of ancillary tracers that relate to $FFCO_2$. The best ancillary analogue of fossil CO_2 is likely to be radiocarbon-CO_2 or $^{14}CO_2$. The spatial gradients of $^{14}CO_2$ in the Northern Hemisphere reflect the dilution of radiocarbon-free $FFCO_2$ in radiocarbon rich ambient air. Radiocarbon-CO_2 measurements with sufficiently high precision are however costly and labor intensive and cannot be deployed as routine measurements on a large network of stations, nor be taken with high enough sampling frequency [*Levin et al.*, 2003]. Therefore other anthropogenic tracers are needed with emissions patterns as close as possible to those of fossil CO_2 and which could be measured at relatively moderate costs. *Bakwin et al.* [1998], for example, used carbon monoxide (CO) to subtract the contribution of fossil sources to total CO_2 at tall towers in the United States. *Zondervan and Meijer* [1996] measured the relationship between $^{14}CO_2$ and CO in Netherlands in order to "calibrate" CO as a surrogate for fossil CO_2 during pollution episodes. The underlying idea is here to establish an empirical calibration between the ancillary tracer and fossil CO_2, either locally or regionally, and then apply it to isolate fossil CO_2 from total CO_2 atmospheric observations.

[4] Our goal is to test the capability of different tracers to quantify the distribution of $FFCO_2$ in the atmosphere. These tracers are CO, SF_6 and C_2Cl_4. The reason for testing CO is that it is emitted together with $FFCO_2$ during the combustion of fuels. Complications may arise however from the fact that CO is destroyed by OH with an average lifetime of 2 months whereas fossil CO_2 is inert, and that CO has other sources than $FFCO_2$ (wild fires and oxidation of biogenic hydrocarbons). The reason for testing SF_6 and C_2Cl_4 is that those tracers are anthropogenic, and to first order, their emissions are distributed similarly to those of $FFCO_2$. SF_6 is inert and C_2Cl_4 has an atmospheric lifetime with respect to oxidation by OH of less than 6 months [*Prather et al.*, 2001].

[5] We will proceed in three steps. First, in the absence of systematic $^{14}CO_2$ measurements everywhere to establish the relationship between $FFCO_2$ and ancillary tracers, we use a transport model to map the spatial variations in that relationship in the Northern Hemisphere. Second, we analyze the temporal relationships between modeled $FFCO_2$ and each tracer at two tall tower stations in the United States, where continuous observations of the tracers exist and can be used to verify the model predictions. Third, based on model results, we estimate the different errors associated with the use of tracers to isolate the fossil fuel component of CO_2. After describing the transport model and the emission maps (section 3), we map the regression slopes between $FFCO_2$ and each ancillary tracer (section 4). In section 5, we investigate the temporal variability of the correlation between fossil CO_2 and tracers on synoptic timescales at two tall tower sites in North Carolina (WITN) and Wisconsin (WLEF). We use actual in situ tracer data to compare them to model results. In section 6, we discuss the different errors associated with the proxy tracer method to estimate $FFCO_2$ from model-derived regressions.

2. Problem

[6] Critical to using ancillary tracers for quantifying the fossil fuel component of CO_2 is the error introduced in the method. Let X_t be the observed CO_2 concentration at a station, X_f the unknown fossil fuel component, and X_a the measured tracer concentration. One can write that

$$X_t = X_f + X_r, \tag{1}$$

where X_r is the "residual" CO_2 concentration from the terrestrial and oceanic surface fluxes. We seek to determine X_r, for instance for inverting its gradients into regional natural sources and sinks. A common way to do this is to model X_f at each site, and replace unknown X_f by a simulated value X_{mf}. The model bias versus reality is unknown, but a lower bound to model error of X_{mf} can be approximated from the spread of different transport model realizations. The TRANSCOM3 project compared 13 global transport models using the same prescribed emission maps of $FFCO_2$. Results showed differences on monthly mean X_{mf} concentrations of up to 3 ppm at Northern Hemisphere atmospheric stations.

[7] For using an ancillary tracer to isolate the fossil CO_2 component, we consider that the sources of X_a and those of fossil CO_2 are reasonably collocated and proportional to each other. The atmospheric transport and chemistry processes will thus also produce roughly proportional concentration fields. Hence one can deduce X_f from X_a with a linear model, rewriting equation (1) as

$$X_t = X_r + S(x,t)X_a, \tag{2}$$

where X_a is the measured concentration of the ancillary tracer, and S the regression slope between tracer and fossil CO_2. Ideally, one would need to know an "instantaneous" slope value $S(x,t)$ at each site and each time, which is impossible to obtain by observations. A reasonable hypothesis is that experimentalists can measure the slope S for example on a few episodes, at a few representative stations, and then extrapolate the value of S to isolate fossil CO_2 elsewhere. A coarser method is to determine S from the ratio of inventoried emissions, and then assume that S is conserved in the transport process. This latter assumption would work only if the X_f to X_a emissions ratio was uniform in space and time, and if X_a is a passive tracer.

[8] We present here a model-based design study for quantifying $S(x, t)$ and evaluating the different errors in isolating fossil CO_2 using an ancillary tracer. The sources of errors that we aim to quantify relate to the spatial variability of $S(x, t)$ in the atmosphere, to the temporal variability of $S(x, t)$, to uncertainties in S and to measurement errors in X_a (see equation (1)). Given that, we can assess whether the tracer based approach is more valuable than using a model to transport fossil emissions and separate X_f, as done in current inversions. We investigate the use of CO, SF_6, and C_2Cl_4, all being routinely measured together with CO_2, either on a continuous basis at a few sites in the United States, or at many more flask sampling sites. To do so, we

model the time varying concentration of these tracers and of fossil CO_2 using an atmospheric chemistry transport model. We first model the variations of S over the Northern Hemisphere. Second, we model the variability of S at two tall tower sites in the United States where the model can be evaluated against in situ CO, SF_6 and C_2Cl_4 observations. The modeled deviations from an idealized perfect linear relationship between X_a and X_f are used to evaluate uncertainties in S, and from there, uncertainties in the overall inference of the fossil CO_2 using modeled slopes and measured CO, SF_6 and C_2Cl_4 concentrations.

3. Modeling Framework

3.1. Atmospheric Chemistry Transport Model

[9] We model the time-varying concentrations of fossil CO_2 CO, SF_6, and C_2Cl_4 taking into account transport and, if necessary, OH chemistry. To that list, we add a conceptual tracer called pC_2Cl_4, which has the same sources as C_2Cl_4, but remains chemically inert in the model. We use the LMD_Z-INCA transport model. LMD_Z is an atmospheric general circulation model developed initially for climate studies [*Sadourny and Laval*, 1984]. The model has been adapted in order to simulate the transport of trace species [*Hourdin and Armengaud*, 1999] and it is coupled online to the chemistry aerosols model: Interaction with Chemistry and Aerosols (INCA). A detailed description and evaluation of the LMD_Z-INCA model is given by *Hauglustaine et al.* [2004]. Model intercomparison involving LMD_Z-INCA can be found in the work of *Bauer et al.* [2004], *Brunner et al.* [2003, 2005], *Guibert et al.* [2005], and *Roelofs et al.* [2003].

[10] We use an online version of the LMDz-INCA with 19 hybrid levels from the surface up to 3 hPa. The vertical resolution is of about 300–500 m in the planetary boundary layer (first level at 70 m height). The model horizontal resolution is 2.5° in latitude and 3.75° in longitude. The large-scale advection of tracers is performed using the finite volume transport scheme of *Van Leer* [1977] as described by *Hourdin and Armengaud* [1999]. Convective transport is simulated using the mass flux scheme of *Tiedtke* [1989]. The planetary boundary layer scheme is based on a second-order closure approximation. The horizontal model winds are relaxed toward ECMWF reanalyzed winds (nudged) with a relaxation time of 2.5 hours.

[11] The version of the INCA chemical scheme used in this study describes the methane oxidation cycle including 19 photochemical reactions and 62 chemical reactions. The INCA module calculates online the time evolution of 33 species with a time step of 20 min. In the present version of the model, nonmethane hydrocarbons and the feedback of the chemistry on the radiation are not taken into account. *Hauglustaine et al.* [2004] evaluated the transport chemistry model against different sets of observations, and concluded that OH was overestimated in the model by 19% to 25% due to these limitations. We carry out a 1 year spin-up for the LMD_Z-INCA chemistry transport model before producing mixing ratio output. The analysis is made for an arbitrary year (1998).

3.2. Surface Emissions

[12] Surface $FFCO_2$ emissions are from the EDGAR version 3.2 inventory for year 1995 [*Olivier and Berdowski*, 2001]. $FFCO_2$ is injected in the lowest box of the atmosphere model (0–140 m). These emissions have no diurnal and no seasonal variation, although we know that, over some regions, there is a seasonality, on the order of 20% in some regions in Germany and of 15% over the United States, for example [*Levin et al.*, 2001; *Blasing et al.*, 2005], due to different use of fossil fuels for heating or air conditioning.

[13] Surface or near surface sources of CO are the sum of fossil fuel and technological biofuel combustion, biomass burning and nonmethane hydrocarbons oxidation. We use fossil fuel CO emissions for year 1995 from EDGAR version 3.2 with global emissions rescaled to the global inventoried totals of 1998 given by *Prather et al.* [2001]. Since nonmethane hydrocarbons (NMHC) are not explicitly included in our chemistry transport model, secondary CO produced by these short-lived species is treated as a surface source, as by *Shindell et al.* [2001]. The global amount of secondary CO produced by NMHC is taken from *Prather et al.* [2001] and distributed with the pattern of the EDGAR 3.2 fossil CO emissions for anthropogenic NMHC and with the pattern of *Guenther et al.* [1995] isoprene emissions for biogenic NMHC. The ratio of secondary CO over primary CO emissions is ≈30%. Biomass burning CO emissions are based on emission factors compiled by *Andreae and Merlet* [2001], and fire distributions of *Hao and Liu* [1994] in the tropics and of *Müller* [1992] in the extratropics. The spatial and temporal distribution of CO oceanic emissions is taken from *Erickson and Taylor* [1992] and scaled to a global mean of 50 Tg CO/yr. More information on the prescribed CO emissions can be found in the work of *Hauglustaine et al.* [2004].

[14] The SF_6 emissions are geographically distributed according to electrical power usage estimated from the UN Energy statistics yearbook 1992 by country and population density (5′ population map of CIESIN). A major source of SF_6 is its use as a dielectric insulator in high-voltage electrical switches. We scale the global mean SF_6 emission total to a global yearly value of 5.686 Gg/yr given by *Levin and Hesshaimer* [1996], and assumed no seasonal cycle of emissions.

[15] The C_2Cl_4 emission map was originally created for year 1990, based upon regional sales data available on a continental scale, national gross domestic products, and population density patterns. C_2Cl_4 is used as a dry cleaning agent in industrial and commercial activities, and it has an atmospheric lifetime with respect to oxidation by OH of less than 6 months [*Prather et al.*, 2001]. Since C_2Cl_4 emissions have been declining after the Montreal Protocol, we scaled globally the 1990 emissions by a factor of 0.82 to extrapolate the global emission inventory for year 1998 following the linear curve given by *McCulloch et al.* [1999]. The C_2Cl_4 emissions are assumed to be temporally invariant over each grid point. In the chemistry transport model we let C_2Cl_4 be oxidized by OH at the rate $k = K_o \exp(-1200/T)$ with $K_o = 9.4 \times 10^{-12}$ cm^3/(mol s) [*De More et al.*, 1997].

4. Mapping: Spatial Variations in the Ratios of Fossil CO_2 to the Ancillary Tracers

4.1. Mapping the Ratios of Emissions

[16] We show in Figures 1b–1d the spatial distribution of the normalized ratios $\rho(x,y)$ of the emissions of fossil CO_2 to

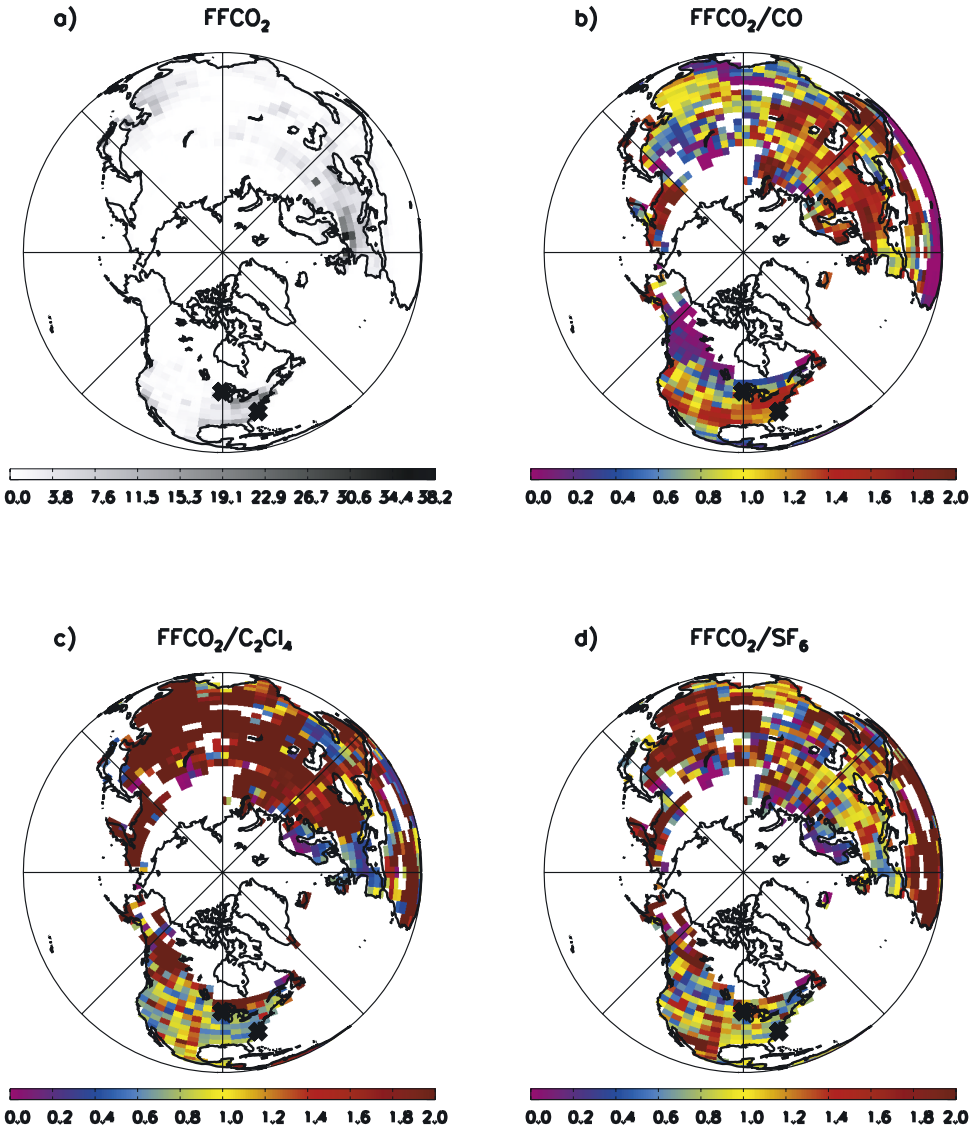

Figure 1. (a) $FFCO_2$ emission map. Units are 1.10^9 mol/m_2/s. (b–d) Normalized ratios ρ_i as defined in the text, where i = CO (Figure 1b), C_2Cl_4 (Figure 1c), and SF_6 (Figure 1d). The ρ_i are ratios of the sources of $FFCO_2$ to CO, C_2Cl_4, and SF_6 normalized by the North Hemisphere totals so that they can be compared to one. The ratios are saturated at a value of 2. These figures exhibit spatial differences in the emissions maps between $FFCO_2$ and the surrogate tracers.

each tracer normalized. For CO emissions, we used the sum of primary sources only. The normalized ratio in each grid point of the Northern Hemisphere is defined by

$$\rho_i = \left(F_f(x,y) / \sum_{\mathrm{NH}} F_f \right) \Big/ \left(F_i(x,y) / \sum_{\mathrm{NH}} F_i \right), \qquad (3)$$

where F_i (x, y) is the emission of the tracer i on grid point (x, y) and F_f (x, y) the emission of fossil CO_2 at the same location. With the normalization, one would have uniform values of ρ $(x, y) = 1$ everywhere for a tracer with emissions perfectly collocated with those of fossil CO_2. Spatial patterns in ρ as shown in Figures 1b–1d indicate regional deviations from the average Northern Hemisphere emission ratio of fossil CO_2 for each tracer emissions. Once transported, such deviations induce spatial and temporal variations in the correlations between the mixing ratios of tracers and fossil CO_2. In Figure 1, the ratios of CO, SF_6 or C_2Cl_4 to fossil CO_2 emissions have, over the United States, a spread between the lowest ($\rho \approx 0.4$) and highest ($\rho \approx 1.9$) values of ρ that is less than on other continents (Europe and Asia). The fossil CO_2 to C_2Cl_4 ratios show over Europe an interesting pattern with higher values of ($\rho \approx 1.9$) in the east and lower values in the west ($\rho \approx 0.3$). The rest of Eurasia has values of the fossil CO_2 to C_2Cl_4 ratios greater than one (Figure 1c). The fossil CO_2 to SF_6 ratio map shows contrasting differences between China ($\rho \approx 2$) and India where the values are closer to one (Figure 1d). The fossil CO_2 to primary CO sources ratios in Figure 1b show low values ($\rho \approx 0.2$) in the tropics and in boreal regions due to biomass burning sources which rise the flux of CO without

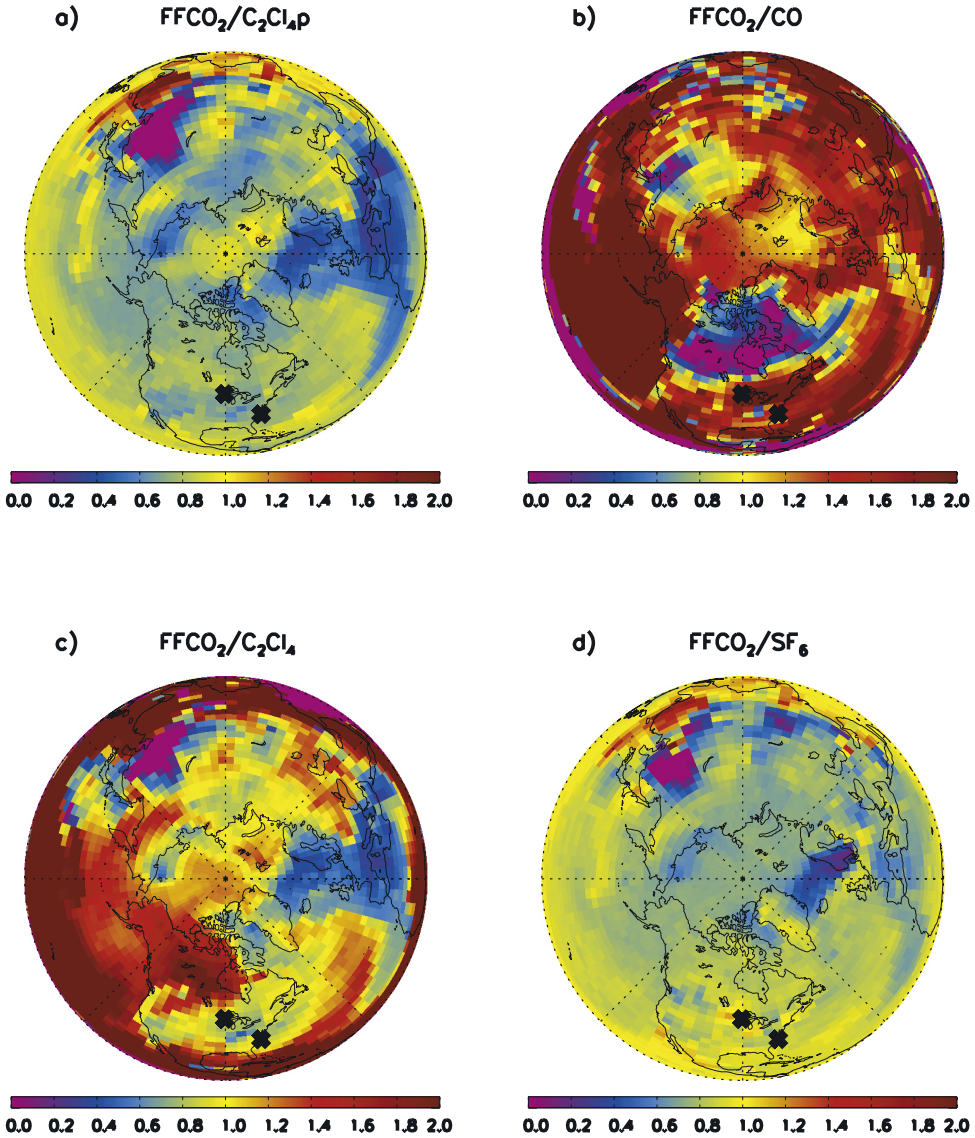

Figure 2. Map of the normalized autocorrelation regression slopes relating the four surrogate tracers SF_6, CO, C_2Cl_4, and pC_2Cl_4 to $FFCO_2$ for the month of August.

changing fossil CO_2 fluxes. Ratios of $FFCO_2$ to CO emissions are however fairly uniform over Europe and the United States.

4.2. Mapping the Ratios of Concentrations

[17] We sampled the model simulated total CO, C_2Cl_4, SF_6 and $FFCO_2$ fields at a time step of 20 min over each grid point. We performed linear regression of the ancillary tracer concentrations against $FFCO_2$ for each month. In calculating linear regression slopes for time series that are serially correlated, we accounted for autocorrelation in time, using the time domain analysis of *Bakwin et al.* [1997, method 4]. This provides more realistic uncertainty estimates than if atmospheric variability is assumed uncorrelated. The autocorrelative regression slopes between the concentrations of tracer, X_i and X_f, are computed using

$$\bar{S}_{fi} = \frac{\bar{C}_{fi} + dc_{fi}}{\bar{C}_{ii} + dc_{ii}}, \tag{4}$$

where C_{fi} is the covariance between tracers i and fossil CO_2 at time lag of Δ, as given by

$$C_{fi}(\Delta) = \sum_t \hat{X}_f(t) Y_i(t + \Delta), \tag{5}$$

where $Y_i(t)$ is the detrended concentration time series with diurnal and seasonal cycles removed, normalized by emissions over the Northern Hemisphere and $\hat{X}_f(t)$ is the time series of simulated fossil CO_2. The overbar indicates averaging over Δ = 4–30 hours. The terms dc_{fi} are each 1000 random values selected from a normal distribution with mean zero and a standard deviation equal to the standard deviations between lags 61–480 hours of the covariance of the time series at the given point.

[18] The autocorrelative slopes are mapped in Figure 2 for August and in Figure 3 for December. We can compare concentration regression slopes (Figure 2) with emission ratios (Figure 1) between fossil CO_2 and ancillary tracers.

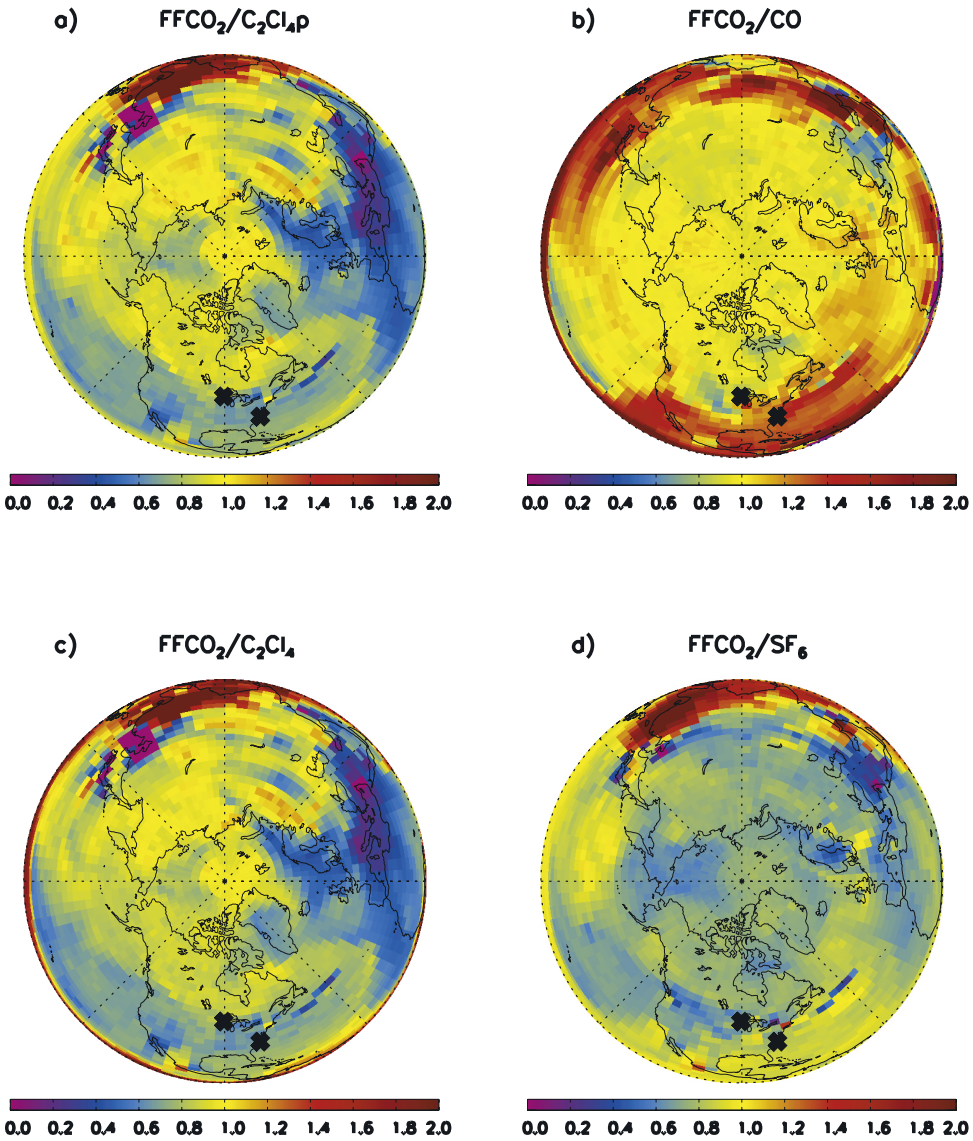

Figure 3. Same as Figure 2 but for the month of December.

Different scales of coherence are seen between the two maps, with concentration regression slopes being spatially coherent at scales of 5000 km versus a few hundred km for the emission ratio maps. In August, higher OH concentrations decrease CO and C_2Cl_4 concentrations relative to $FFCO_2$ and thus make the slopes higher than in December. The average slopes and their standard deviation over the United States, North Atlantic and Europe are given in Table 1. We found the largest spatial gradients in the slope in summer and for the chemically active species (Table 1). The August spatial gradients of $FFCO_2$ versus CO and C_2Cl_4 slopes are two times smaller over Europe than over North America, reflecting the spatial structure of underlying emission ratios (Figure 1). Comparing in Figures 2a–2c the slopes for C_2Cl_4 and pC_2Cl_4 shows the influence of chemistry in summer. Chemistry induces on average, four times

Table 1. Mean and Standard Deviation of the Slopes Between Tracers and Fossil CO_2 Over North America, North Atlantic, and Europe in January and August

	North America		North Atlantic		Europe	
	Jan	Aug	Jan	Aug	Jan	Aug
CO	1.3 (0.2)	1.5 (0.7)	1.3 (0.2)	1.6 (0.6)	1.0 (0.1)	1.5 (0.3)
SF_6	0.8 (0.2)	0.8 (0.1)	0.8 (0.1)	0.8 (0.1)	0.7 (0.1)	0.7 (0.1)
C_2Cl_4	0.7 (0.2)	1.1 (0.5)	0.7 (0.1)	1.2 (0.6)	0.6 (0.2)	0.9 (0.3)
pC_2Cl_4	0.7 (0.1)	0.8 (0.1)	0.7 (0.1)	0.8 (0.1)	0.6 (0.2)	0.7 (0.2)

larger spatial gradients in the $FFCO_2$ versus C_2Cl_4 slopes compared to the $FFCO_2$ versus pC_2Cl_4 ones.

5. Mapping Temporal Variations in the Correlations of Tracers $FFCO_2$ Versus the Tracers at Two Tall Towers in the United States

[19] In this section, we further analyze correlation between ancillary tracers and $FFCO_2$ at two tall tower sites where in situ tracer observations exist. Doing so, we still rely on model calculations of fossil CO_2, but we can now evaluate the modeled tracer concentrations against real observations.

5.1. Tall Tower Measurements in North Carolina and Wisconsin

[20] Tracer data are from the North Carolina (WITN) and Wisconsin (WLEF) tall towers operated by NOAA/CMDL. The WITN tower is 610 m tall, located in a rural area of the eastern United States at 35.37°N, 77.39°W, relatively close, to industrialized regions of the east coast. The WLEF tower is 447 m tall and is located in a forested and sparsely populated region of northern Wisconsin at 45.95°N, 90.27°W, 472 m asl [*Bakwin et al.*, 1995, 1998]. Of particular interest is the contrast of population around the two towers, with 64 persons km^{-2} at WITN and 5 persons km^{-2} at WLEF (typical density of regions within 50 km or more of the towers) [*Bakwin et al.*, 1998]. Generally, the WLEF tower samples air masses containing the integrated signals of distant source regions, mixed with cleaner regional background air, whereas the WITN tower is more immediately influenced by anthropic emissions.

[21] Measurements of CO, SF_6, and C_2Cl_4 were made by automated, in situ gas chromatography, on an hourly basis. Measurement precision is about 4 ppb for CO, 0.03 ppt for SF_6, and 0.2 ppt for C_2Cl_4 [*Hurst et al.*, 1997; *Bakwin et al.*, 1997]. Tracer data used here were collected at 51 m at the WITN, and 30 m at WLEF. Data from the North Carolina tower have been analyzed by *Hurst et al.* [1997, 1998] and *Bakwin et al.* [1997] who found strong correlations on synoptic timescales between C_2Cl_4, CO and SF_6. At both tall tower sites, continuous records of CO, SF_6, and C_2Cl_4 are most useful to evaluate the LMD_Z-INCA model performance for synoptic variability. A realistic transport model on those timescales is a prerequisite to investigate temporal variations in the regression slopes between tracers and fossil CO_2 and select those tracers which have the tighter relationship with fossil CO_2, and could be used in inversions to separate that component of CO_2.

5.2. Variability of the Fossil CO_2 Versus Tracer Scatterplots

[22] In Figures 4 and 5, we show fossil CO_2 versus each modeled tracers regression plots in August and December. At WITN, we find a tighter correlation for both winter and summer than at WLEF. This is likely due to the fact that there is a good collocation among the proximate sources of all species. Relying on the model to evaluate tracers for isolating fossil CO_2, this result clearly indicates that the method to establish a proxy for fossil CO_2 tends to be site specific. Generally better correlations will be expected at sites downwind from emission regions. At face value, we expect any tight relationship between $FFCO_2$ and tracers to degrade if a station is placed very close to a source region (i.e., in a city) because of averaging at the grid level. Indeed, *Gerbig et al.* [2003] showed that past a model grid size of 30 km the representation error (due to averaging of the subgrid variability) greatly dominates the actual sampling error (coming from the atmospheric variance) of CO_2 measurements. Thus variance induced by the close proximity of the sources will not be captured in a global transport model such as LMD_Z-INCA but rather will increase the representation error.

[23] In summer at WITN (Figure 5), SF_6 is the modeled tracer with the highest correlation coefficient with fossil CO2 (R^2 = 0.997). The second best correlation with fossil CO_2 is found with C_2Cl_4 (R^2 = 0.981). We obtain a lower correlation than for SF_6, due to the removal of C_2Cl_4 by OH. The conceptual passive tracer (pC_2Cl_4), exhibits in contrast a correlation with fossil CO_2 of 0.996, equally as good as for SF_6. In August, scatter around the linear fit to the regression of C_2Cl_4 versus fossil CO_2 in Figure 5 owes to the fact that each ''polluted'' air mass carries a distinct ratio between C_2Cl_4 and fossil CO_2, with OH increasing the fossil CO_2 to C_2Cl_4 ratio. Finally, CO shows the worst correlation with fossil CO_2 (R^2 = 0.905). This occurs because CO is destroyed by OH, and CO has sources not collocated with fossil CO_2 emissions, such as biomass burning and production from NMHC. The same conclusions relative to which tracer best approximates fossil CO_2 also hold at the WLEF tall tower. In Wisconsin, the correlation of CO versus fossil CO_2 (R^2 = 0.805) is lower than in North Carolina (R^2 = 0.905). The WLEF tower is reached in summer by air masses with elevated CO originating from wildfires in Canada and the western United States and low fossil CO_2 concentrations. For both tower sites, the modeled correlations between CO, C_2Cl_4 and fossil CO_2 are higher in December than in August. This is primarily due to inhibited OH chemistry increasing the lifetime of active tracers. In fact, we find that in December, all ancillary tracers SF_6, C_2Cl_4 and CO are about equally as good indicators of the presence of fossil CO_2. *Potosnak et al.* [1999] reached to a similar conclusion for CO and fossil CO_2, based on atmospheric records from the Harvard Forest (Massachusetts). At WLEF, the winter correlations between any tracer and fossil CO_2 are always lower than at WITN in North Carolina. Located closer to anthropogenic emissions, the WITN tower remains more consistently influenced by regional emissions from the east coast. We recall from Figure 1 that different industrialized regions of the Northern Hemisphere have SF_6 to fossil CO_2 emission ratios that can vary by a factor of two. In winter, the signals from those different regions get mixed by fast longitudinal transport, and no unambiguous surrogate tracer of fossil CO_2 can be obtained. This is a major limitation of using tracers to isolate the fossil fuel signal in the CO_2 concentration field, which has been overlooked when using for example, a slope simply derived from regional emission inventories [*Bakwin et al.*, 1995].

5.3. Variability of the Fossil CO_2 Versus Tracer Regression Slopes

[24] The monthly linear regression slope of fossil CO_2 versus SF_6 remains approximately constant throughout the year at both towers (Figure 6). This indicates that, according

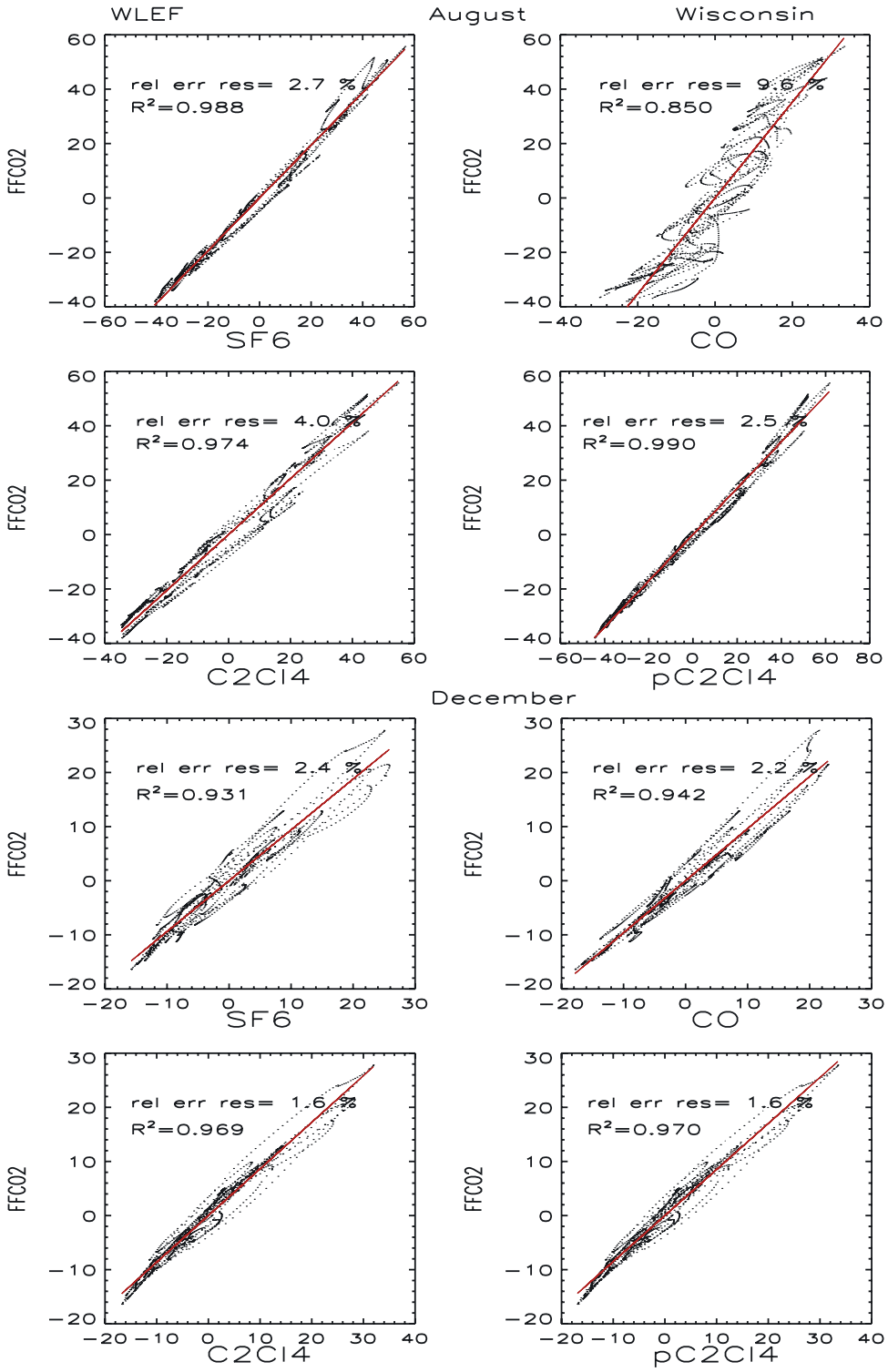

Figure 4. Regression in August and December 1998 at WLEF (Wisconsin) between simulated $FFCO_2$ mixing ratios on the *y* axis and the normalized mixing ratios of SF_6, CO, C_2Cl_4, and pC_2Cl_4 (same as C_2Cl_4 but without OH destruction), respectively, on the *x* axis. The monthly averaged value is subtracted for all quantities.

to our model, SF_6 should be both a spatially and temporally robust proxy for fossil CO_2. The SF_6 versus fossil CO_2 slope is close to 1 at WITN and equal to 0.9 at WLEF, a difference which can be explained by the larger influence of remote sources at WLEF, characterized by lower $FFCO_2$ to SF_6 ratios.

[25] The monthly slope between C_2Cl_4 and fossil CO_2 is not constant throughout the year, as is the case for SF_6. This

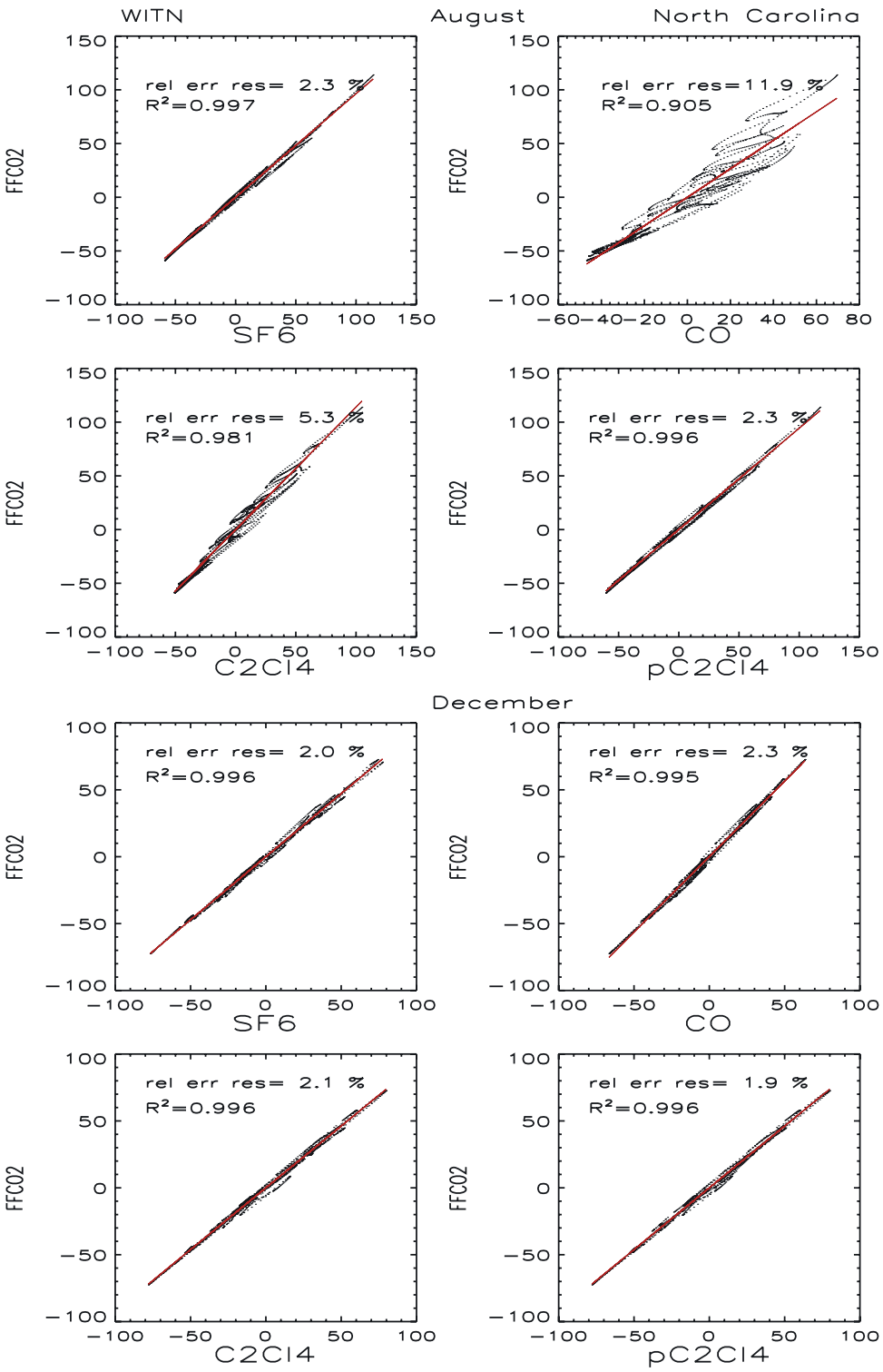

Figure 5. Same as Figure 4 but at WITN (North Carolina).

is mainly because C_2Cl_4 is affected by reaction with OH, as can be inferred from comparison between pC_2Cl_4 and C_2Cl_4. In Figure 6 at WLEF, the comparison between the pC_2Cl_4 and C_2Cl_4 slopes shows that the oxidation by OH changes the slopes from being equal in winter to differ by 15% over the summer months when OH photochemical production is maximum (the difference is slightly less ~10% at WITN due to the closer proximity to the sources). This raises a caution flag if C_2Cl_4 is to be used like a passive tracer for isolating the fossil CO_2 component. Oxidation by OH tends to make the fossil CO_2 versus C_2Cl_4 slope higher than the fossil CO_2 versus pC_2Cl_4 slope. Similarly to SF_6, we found that the fossil CO_2 versus C_2Cl_4 normalized slope is lower at WLEF, owing to dilution of air masses of

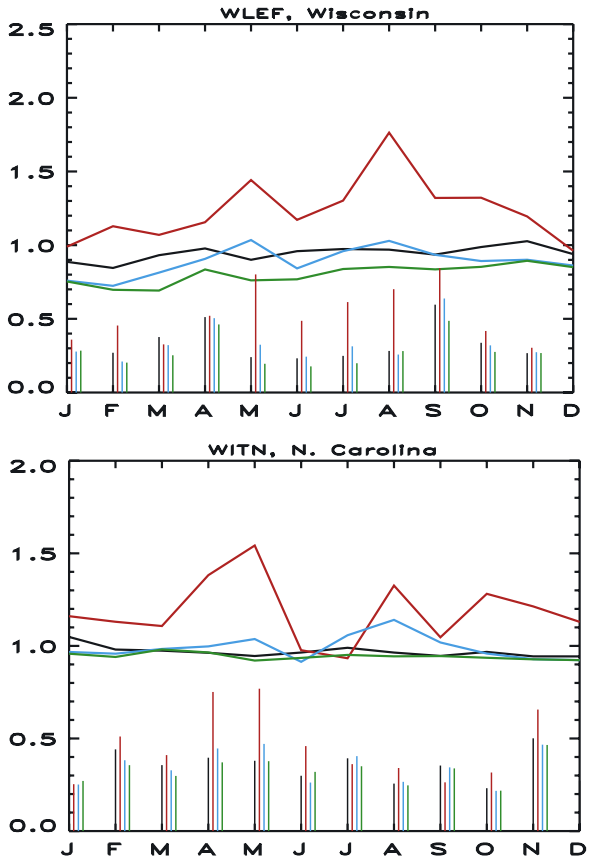

Figure 6. Monthly normalized regression slopes for WLEF (Wisconsin) and WITN (North Carolina) computed when accounting for autocorrelations in time series (see text). A perfect proxy of $FFCO_2$ should have at any month a slope close to 1. In black are the SF_6-$FFCO_2$ slopes, in red are the CO-$FFCO_2$ slopes, in blue are the C_2Cl_4-$FFCO_2$ slopes, and in green are the C_2Cl_4p-$FFCO_2$ slopes. Error bars shown at the bottom of the plot correspond to half the range between the 16th and 84th percentiles of the Monte Carlo estimates of the slopes (see text).

different origin into background air containing more C_2Cl_4 in proportion to $FFCO_2$. For chemically reactive species, differences among sites can be explained both by differences in exposure to OH (more OH increases the slope), and by differences in mixing with background air (more dilution with background air high in C_2Cl_4 decreases the slope).

[26] The monthly regression slope of fossil CO_2 versus CO is on average 20% higher than the idealized value of 1 if both tracers had identical sources and transport. Other primary sources of CO than fossil fuel combustion would otherwise tend to decrease the fossil CO_2 versus CO slope. Our results indicate that the effect of photochemical destruction of CO is more important in controlling the value of the slope. In addition, the effect of OH is proportionally larger on the fossil CO_2 versus CO slope than on that for fossil CO_2 versus C_2Cl_4 because CO has a shorter lifetime than C_2Cl_4. This hinders the use of an annually constant slope for using CO to subtract the fossil component of CO_2 observations in North America. Using a slope value predicted by a chemistry transport model might be a feasible alternative, provided that the model performs well in reproducing the variations of CO. Inspecting the monthly linear correlation coefficient of fossil CO_2 versus CO in the model shows that CO may be safely used to approximate fossil CO_2 between October and February, but that it is not a reliable proxy during the rest of the year. Comparing the correlation coefficients values at WLEF and WITN does not favor either station.

5.4. Modeled Variance of Tracers

[27] Deducing $FFCO_2$ from ancillary tracers using model derived regression slopes, raises the key question of whether or not the model captures the variability of actual tracer data. In the next section, we compare modeled and observed tracer concentrations at the two tall towers and discuss the implications of model-data mismatch for determining the fossil CO_2 component.

[28] Modeled and observed tracers time series for the year 1998 are shown in Figure 7 (WITN) and Figure 8 (WLEF). At both towers, a seasonal cycle for CO and C_2Cl_4 is present, but weaker at WITN. WITN lies closer to the sources so that CO and C_2Cl_4 are less oxidized by OH. In contrast to CO and C_2Cl_4, SF_6 does not show any seasonal cycle. There is no seasonality prescribed to the emissions of C_2Cl_4, thus the modeled C_2Cl_4 seasonal cycle only reflects transport and varying OH concentrations. This is not the case for CO, which has a biomass burning component maximum in summer [*Hao and Liu*, 1994]. The proximity of anthropogenic sources explains why there is a greater variability at WITN than at WLEF both in the model and in the observations (Table 2).

[29] Synoptic variability is an important determinant of the value of the slopes. Thus it is important to show that the model correctly captures this mode of variability. Figure 9 displays tracer changes during the first 3 months of 1998 at WITN. Most synoptic events appear well correlated across all tracers suggesting good collocation of the sources for these compounds. Figure 9 shows good (>0.5) correlation between model and data for CO and C_2Cl_4 but the magnitude and the phase of SF_6 changes are not well captured.

[30] We compare in Table 2 the modeled and observed tracer variability, in standard deviation of hourly values. The model underestimates the observed standard deviation by a factor four for SF_6 at both towers whereas the simulated CO and C_2Cl_4 are realistic. These results for SF_6 should not reduce our confidence in the model which works well for CO and C_2Cl_4.

[31] Compared to the model intercomparison of *Denning et al.* [1999] (Figure 8), the LMD_Z simulated variability measured as the difference between the third and first quartile is 0.21 ppt for WITN and 0.14 ppt for WLEF which puts LMD_Z among the best half of the models. SF_6 mixing ratios seem to be influenced by non inventoried local sources (at least at the two towers). Also the relative measurement error (Table 3) is the largest for SF_6 when compared to CO or C_2Cl_4, which could partly explain why models are less able to capture the hourly variability of SF_6.

[32] In terms of error on the slope, a model underestimation of the variance by a factor of four would propagate into multiplying the error on the slope (cf next section) by the same amount. Unfortunately, this precludes the use of SF_6 and model-derived slopes to determine $FFCO_2$, even though

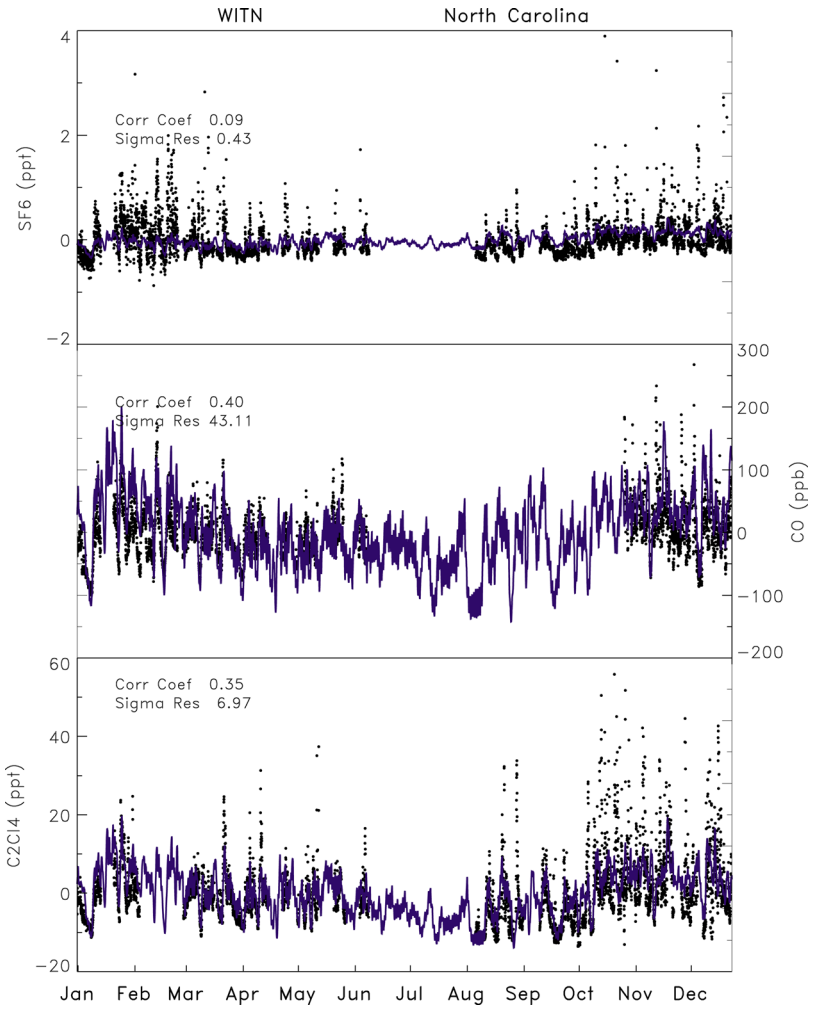

Figure 7. Comparison between the observed (black dots) and the modeled (blue line) mixing ratios at WITN in North Carolina during 1998. The annual average is subtracted from both time series. The observations were made at an altitude of 51 m above ground. The modeled time series is extracted out of the model at an interpolated height of 50 m. Observed/modeled correlation coefficients and residual standard deviation are given for all tracers.

in the model realm, the SF_6 slopes were found the most robust (see section 4.3).

6. Analysis of Errors and Discussion

[33] To further assess the accuracy of the method by which fossil CO_2, X_f can be deduced from a tracer X_a by $X_f = SX_a$ (see equations (1) and (2)), we give in Table 3 the measurement error on X_a and the uncertainty on the slope S at both tower locations.

[34] The reported measurement errors for each tracers are relative errors, (instrument precision errors divided by observed standard deviation of each species). Care has to be taken in computing uncertainties in the slope S in the model. The concentrations being autocorrelated in time, a simple RMS fit error from the linear fit X_f versus X_a would greatly underestimate the true error as can be seen in Table 3, by comparing the RMS fit error and the slope uncertainty. In Table 3, slope uncertainty values are determined as half the range between the 16th and 84th percentiles of the Monte Carlo estimates of the slopes computed using equation (4) (uncertainty bars shown at the bottom of Figure 6). It is important to keep in mind that our slope uncertainty which accounts for serial correlation in the time series, is related to variability not explained by the correlations and gives more reliable uncertainty estimates than other methods [*Bakwin et al.*, 1997]. The uncertainty on the slope of the order 30 to 40% is clearly the dominant source of error in the approximation $X_f = SX_a$. The measurement errors are always at least a factor two smaller than the uncertainty on the slope.

[35] Other systematic errors enter in the tracer approximation of $FFCO_2$. Emission fluxes are biased by aggregation errors in space and time. However, aggregation errors associated with tightly constrained spatial patterns in the emission maps may cancel since similar aggregation errors are likely to bias $FFCO_2$ and anthropogenic tracer emissions. To evaluate the impact of seasonality in $FFCO_2$ emissions slopes, we performed the same model analysis using a $FFCO_2$ emission map with a prescribed peak to peak seasonality of 20% in the Northern Hemisphere (maximum emissions in winter). Results of this test for

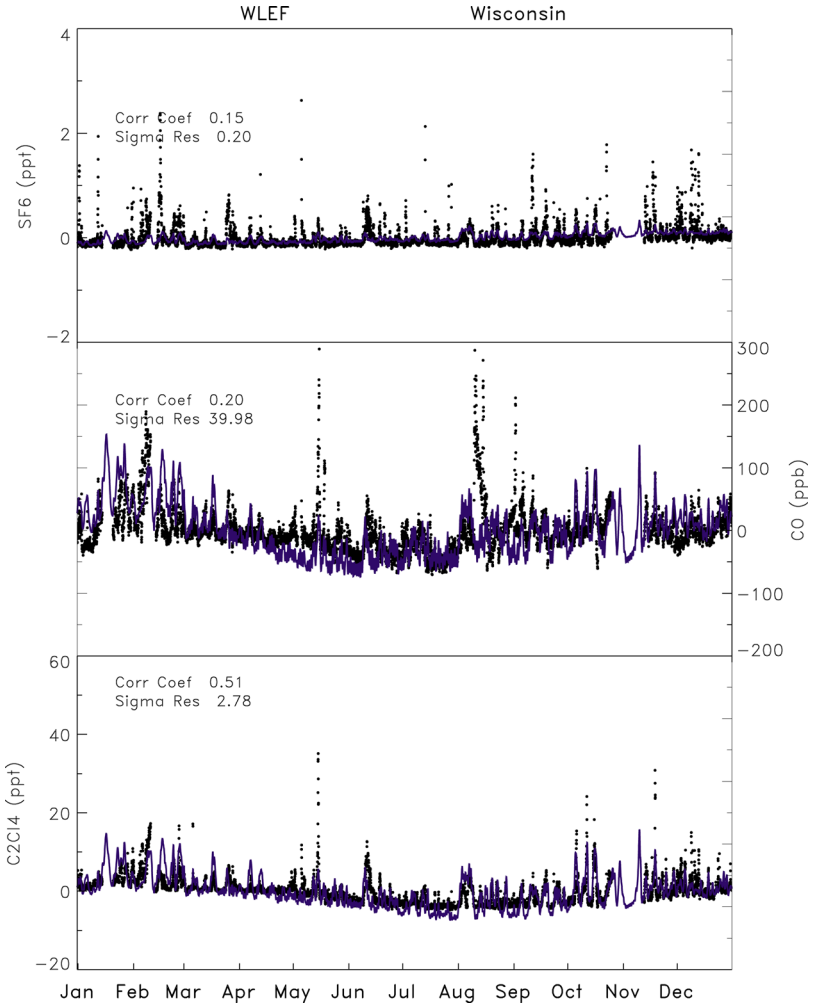

Figure 8. Same as Figure 7 but at WLEF. Monthly normalized regression slopes for WLEF (Wisconsin) and WITN (North Carolina) computed when accounting for autocorrelations in time series (see text). A perfect proxy of $FFCO_2$ should have at any month a slope close to 1. In black are the SF_6-$FFCO_2$ slopes, in red are the CO-$FFCO_2$ slopes, in blue are the C_2Cl_4-$FFCO_2$ slopes, and in green are the C_2Cl_4p-$FFCO_2$ slopes. Error bars shown at the bottom of the plot correspond to half the range between the 16th and 84th percentiles of the Monte Carlo estimates of the slopes (see text).

the two tall towers (not shown) showed a reduction of the modeled slopes in summer and an overall annual bias of 20% when compared with the case of invariant sources of $FFCO_2$.

[36] This analysis of the uncertainty associated with the ancillary tracer method is important in assessing its practical use. The "standard method" in CO_2 inversions is to subtract the fossil fuel component of the CO_2 concentration at stations out of the observed CO_2. The fossil CO_2 component is estimated using one particular emission inventory maps and one particular transport model. The inversion then solves for "residual" oceanic and terrestrial fluxes. The strategy in using a tracer method consists in deriving fossil fuel concentrations from tracers observations with modeled slopes. We showed that the main source of uncertainty on the slope S is on the order 30%. In the standard method a large part of the uncertainty is contained in the (unknown) bias of the transport model. Using several models can provide a measure of this error. The spread between different global transport models is on the order of 20% in simulating monthly fossil CO_2 at the two tall towers WLEF and WITN [*Gurney et al.*, 2004]. This is probably a lower bound of the model uncertainty since (1) the same smooth emission map was prescribed to all models and (2) only coarse-scale global models were used. So, the conditions

Table 2. Standard Deviation of the Detrended Time Series and Comparison Between the Observations and the Modeled Time Series[a]

	WLEF		WITN	
	Observed	Modeled	Observed	Modeled
CO	32	24	40	47
SF_6	0.20	0.05	0.43	0.09
C_2Cl_4	2.6	2.8	7.9	4.7

[a]For all species the variability is greater at the WITN (North Carolina) tower. Units are ppt for SF_6 and C_2Cl_4 and ppb for CO.

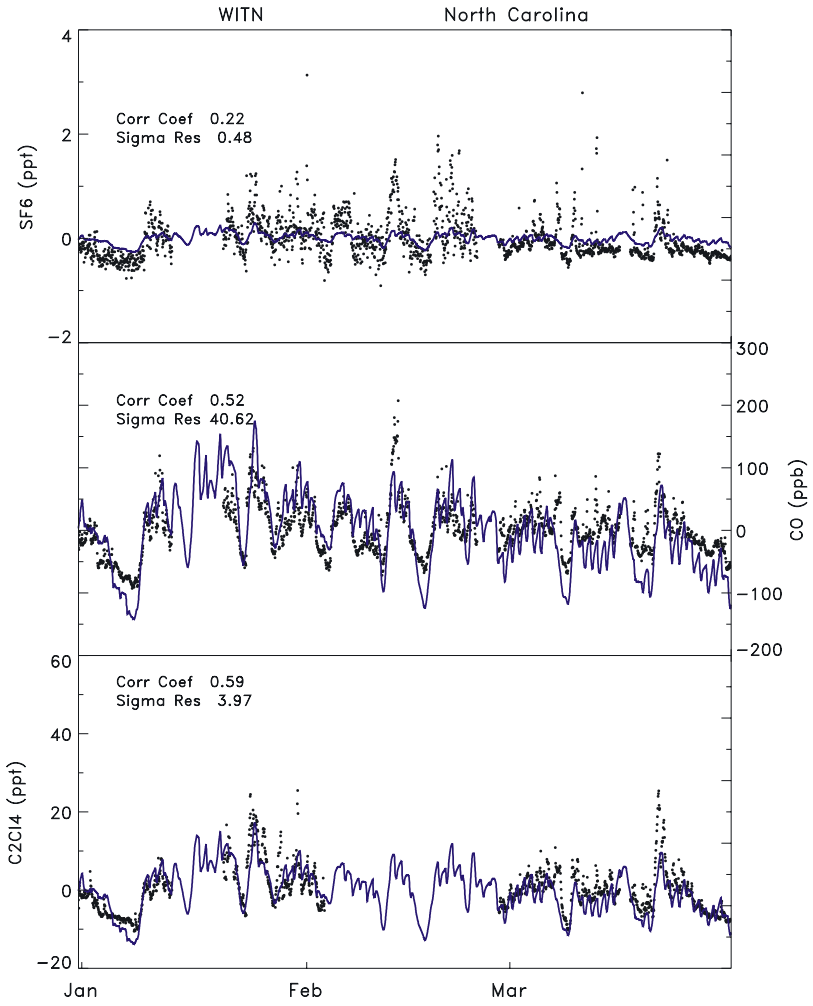

Figure 9. Comparison between the observed (black dots) and the modeled (blue line) mixing ratios at WITN in North Carolina during 1998. The average is subtracted from both time series shown for the months of January, February, and March.

of the intercomparison did not allow to explore all the range of model differences. Error associated with regional patterns in emissions are also expected to be significant. At the national level, for fossil CO_2, total emissions is known with an error of 8% uncertainty, but it can range from −340% to 90% for a given country and year [*Andres et al.*, 1999]. Emissions are obtained by making the product of an emission factor by an activity. There are significant sources of errors due to activity definitions, activity mapping, and to the use of emission factors determined for one region/activity and used for another. Hence the spatial distribution of fossil emissions at regional scales is even more uncertain than country totals. Also, only recently has the seasonality of the emissions and potential associated error been considered in inversions [*Gurney et al.*, 2004]. When using refined fossil fuel emissions, with hourly temporal variation over Europe at a 50 km resolution, it appears that the spread of the model increased significantly (P. Peylin and CarboEurope-IP participants, preliminary results).

[37] The tracer method is likely to be more robust than the standard method. The errors associated with transport and emissions tend to be smaller in the tracer approach since ratios of two tracers are used with the same model (thus canceling some of the modeled transport bias) and using emission sources which can share common biases (e.g., activity distributions). Thus the errors on the ratio used to

Table 3. Relative Errors[a]

	Fit Error			Slope Uncertainty	
	Dec	Aug	Measurement Error	DJF	JJA
			CO		
WLEF	2.2	9.6		41	36
WITN	2.3	11.9	10	32	40
			SF_6		
WLEF	2.4	2.7		45	26
WITN	2	2.3	12	34	32
			C_2Cl_4		
WLEF	1.6	4		45	29
WITN	2.1	5.3	3.5	34	32
			pC_2Cl_4		
WLEF	1.6	2.5		44	25
WITN	1.9	2.3		35	33

[a]Expressed in percent. See text for a description of the different errors.

quantify fossil CO_2 are less impacted by biases than in the standard method.

7. Conclusion

[38] Using an atmospheric chemistry transport model, we simulated the regression slope between fossil CO_2 and the one of anthropogenic tracers CO, SF_6 and C_2Cl_4. One can then use this slope to estimate fossil CO_2 from actual measurement of surrogate tracers. We evaluated the model using actual tracer observations at two tall towers sites in the United States. We estimated the regression slopes variations in the Northern Hemisphere, and the errors in the retrieval of fossil CO_2 based upon anthropogenic tracers.

[39] The fossil CO_2 to CO and C_2Cl_4 ratio is smaller over Europe than over North America, reflecting difference in emissions. The regression slopes show larger spatial variations in summer than in winter for the reactive tracers CO and C_2Cl_4, which reflects their removal by OH radicals. We compared two tall tower sites (WLEF, Wisconsin and WITN, North Carolina) in the United States. We found that differences in the ratio of fossil CO_2 versus tracers between the two sites can be explained both by differences in exposure to OH (more active OH photochemistry increases the ratio), and by differences in their proximity to pollution (more polluted air decreases the ratio). The regression slopes of fossil CO_2 to tracers vary during the year. The largest values occur in summer for the chemically reactive species CO (+25%) and C_2Cl_4 (+15%). This raises a caution flag if C_2Cl_4 or CO are assumed to be passive tracers for retrieving the fossil CO_2 component. At the two tall tower sites, our model results indicate that the effect of CO removal by OH is more important in controlling the value of the slope than mixing with nonanthropogenic CO. In addition, the impact of OH removal on the slope is proportionally larger on the fossil CO_2 versus CO slope than on the fossil CO_2 versus C_2Cl_4 one. This is because CO has a shorter lifetime than C_2Cl_4. In wintertime, all anthropogenic tracers SF_6, C_2Cl_4 and CO are about equally as good proxies of fossil CO_2.

[40] When we compared modeled to observed variance of the mixing ratios, we found that the model underestimates the observed standard deviation by a factor of four for SF_6 at both towers whereas results for CO and C_2Cl_4 are good. We believe that this is due to SF_6 mixing ratios being very dependent on local and point sources (at least for the two towers) that are not included in the model. In the end, this precludes the use of SF_6 in this method at least in comparison to CO and C_2Cl_4 even though in the "modeled world," SF_6 slopes were more robust in terms of time and space variability. Thus among SF_6, CO, C_2Cl_4, we recommend C_2Cl_4 since it has less spatial and time variability than CO and since SF_6 variability is not correctly captured by the model. The uncertainty on the slope S of fossil CO_2 versus tracer, is estimated to be on the order of 30 to 40%. Uncertain S values are the dominant cause of error when retrieving fossil CO_2 from tracer concentration measurements. Traditionally in atmospheric inversions, the fossil CO_2 component is subtracted out of the modeled CO_2 mixing ratio to solve for residual ocean and terrestrial sources and sinks. In that process,. Fossil CO_2 emission inventory maps, input to transport models are used to compute the fossil CO_2 signal. The errors on this approach include transport model errors and emission inventories errors. The spread from 16 different transport models [*Gurney et al.*, 2004] suggests that a lower bound on the transport error is on the order of 20%, but models can all remain biased with respect to the unknown truth. The spread from different emission inventories maps is also likely to be quite large, on the order of 30–40% locally (P. Peylin and Carboeurope-IP participants, preliminary results). Errors on emission inventories are small at global scale but largely increase down to regional scale. In the tracer method studied here, using model-derived slopes, the errors associated with transport or emission inventories will tend to cancel each other since the ratios of two tracers are estimated using the same model and emission maps can share common biases through the distribution of anthropogenic activities. Monthly values of the ratio between fossil CO_2 and each anthropogenic tracer can be of interest for experimentalists who could determine the value these slopes only at a few sites. Information on the space and time variability in the ratios could hence be used to assess the representativeness of slopes measured at a given point. Using tabulated values of these ratios would improve on practices where a constant ratio is used during the whole year as done in the past with CO for example. Finally, a natural follow up of this work is to use the tracer method in inversions to reduce uncertainties on fossil fuel CO_2 fluxes.

References

Andreae, D. J., and P. Merlet (2001), Emissions of trace gases and aerosols from biomass burning, *Global Biogeochem. Cycles*, *15*, 955–966.

Andres, R. J., et al. (1999), Carbon dioxide emissions from fossil-fuel use, 1751–1950, *Tellus, Ser. B*, *51*, 759–765.

Bakwin, P. S., C. Zhao, W. Ussler III, P. P. Tans, and E. Quesnell (1995), Measurements of carbon dioxide on a very tall tower, *Tellus, Ser. B*, *47*, 535–549.

Bakwin, P. S., D. F. Hurst, P. P. Tans, and J. W. Elkins (1997), Anthropogenic sources of halocarbons, sulfur hexafluoride, carbon monoxide, and methane in the southeastern United States, *J. Geophys. Res.*, *102*, 15,915–15,925.

Bakwin, P. S., P. P. Tans, D. F. Hurst, and C. Zhao (1998), Measurements of carbon dioxide on very tall towers: Results of the NOAA/CMDL program, *Tellus, Ser. B*, *50*, 401–415.

Bauer, S. E., Y. Balkanski, M. Schulz, D. A. Hauglustaine, and F. Dentener (2004), Global modeling of heterogeneous chemistry on mineral aerosol surfaces: Influence on tropospheric ozone chemistry and comparison to observations, *J. Geophys. Res.*, *109*, D02304, doi:10.1029/2003JD003868.

Blasing, T. J., C. T. Broniak, and G. Marland (2005), The annual cycle of fossil-fuel carbon dioxide emissions in the United States, *Tellus, Ser. B*, *57*, 107–115.

Brunner, D., et al. (2003), An evaluation of the performance of chemistry transport models by comparison with research aircraft observations. part 1: Concepts and overall model performance, *Atmos. Chem. Phys.*, *3*, 1616–1631.

Brunner, D., et al. (2005), An evaluation of the performance of chemistry transport models. part 2: Detailed comparison with two selected campaigns, *Atmos. Chem. Phys.*, *5*, 107–129.

De More, W. B., et al. (1997), *Chemical Kinetics and Photochemical Data for Use in Stratospheric Modeling*, *Publ. 97-4*, Jet Propul. Lab., Pasadena, Calif.

Denning, A. S., et al. (1999), Three-dimensional transport and concentration of SF6: A model intercomparison study (TransCom 2), *Tellus, Ser. B*, *51*, 266–297.

Erickson, D. J., III, and J. A. Taylor (1992), 3-D tropospheric CO modeling: The possible influence of the ocean, *Geophys. Res. Lett.*, *19*, 1955–1958.

Gerbig, C., J. C. Lin, S. C. Wofsy, B. C. Daube, A. E. Andrews, B. B. Stephens, P. S. Bakwin, and C. A. Grainger (2003), Toward constraining regional-scale fluxes of CO_2 with atmospheric observations over a continent: 1. Observed spatial variability from airborne platforms, *J. Geophys. Res.*, *108*(D24), 4756, doi:10.1029/2002JD003018.

Guenther, A., C. N. Hewitt, T. Pierce, B. Lamb, P. Harley, and R. Fall (1995), A global model of natural volatile organic compound emissions, *J. Geophys. Res.*, *100*, 8873–8892.

Guibert, S., V. Matthias, M. Schulz, J. Bösenberg, R. Eixmann, I. Mattis, G. Pappalardo, M. R. Perrone, N. Spinelli, and G. Vaughan (2005), The vertical distribution of aerosol over Europe—Synthesis of one year of EARLINET aerosol lidar measurements and aerosol transport modeling with LMDzT-INCA, *Atmos. Environ.*, *39*, 2933–2943.

Gurney, K. R., et al. (2004), Transcom 3 inversion intercomparison: Model mean results for the estimation of seasonal carbon sources and sinks, *Global Biogeochem. Cycles*, *18*, GB1010, doi:10.1029/2003GB002111.

Hao, W. M., and M.-H. Liu (1994), Spatial distribution of tropical biomass burning in 1 980 with $5° \times 5°$ resolution, *Global Biogeochem. Cycles*, *8*, 495–503.

Hauglustaine, D. A., F. Hourdin, L. Jourdain, M.-A. Filiberti, S. Walters, J.-F. Lamarque, and E. A. Holland (2004), Interactive chemistry in the Laboratoire de Météorologie Dynamique general circulation model: Description and background tropospheric chemistry evaluation, *J. Geophys. Res.*, *109*, D04314, doi:10.1029/2003JD003957.

Hourdin, F., and A. Armengaud (1999), The use of finite-volume methods for atmospheric advection of trace species. part 1: Test of various formulations in a general circulation model, *Mon. Weather Rev.*, *127*, 822–837.

Hurst, D. F., P. S. Bakwin, R. C. Myers, and J. W. Elkins (1997), Behavior of trace gas mixing ratios at a very tall tower site in North Carolina, *J. Geophys. Res.*, *102*, 8825–8835.

Hurst, D. F., P. S. Bakwin, and J. W. Elkins (1998), Recent trends in the atmospheric variability of halogenated trace gases over the United States, *J. Geophys. Res.*, *103*, 25,229–25,306.

Levin, I., and V. Hesshaimer (1996), Refining of atmospheric transport model entries by the globally observed passive tracer distributions of ^{85}Kr and sulfur hexafluoride (SF_6), *J. Geophys. Res.*, *101*, 16,745–16,755.

Levin, I., B. Kromer, and M. Schmidt (2001), Regional fossil fuel CO_2 fluxes quantified by atmospheric observations: An approach to verification of the Kyoto Protocol, paper presented at the Sixth International Carbon Dioxide Conference, Cent. for Atmos. and Oceanic Stud., Grad. Sch. of Sci., Tohoku Univ., Sendai, Japan, 1–5 Oct.

Levin, I., B. Kromer, M. Schmidt, and H. Sartorius (2003), A novel approach for independent budgeting of fossil fuel CO_2 over Europe by $^{14}CO_2$ observations, *Geophys. Res. Lett.*, *30*(23), 2194, doi:10.1029/2003GL018477.

Marland, G., and R. M. Rotty (1984), Carbon dioxide emissions from fossil fuels: A procedure for estimation and results for 1950–1982, *Tellus, Ser. B*, *36*, 232–261.

McCulloch, A., M. L. Aucott, T. E. Graedel, G. Kleiman, P. M. Midgley, and Y.-F. Li (1999), Industrial emissions of trichloroethene, tetrachloroethene, and dichloromethane: Reactive Chlorine Emissions Inventory, *J. Geophys. Res.*, *104*, 8417–8428.

Müller, J.-F. (1992), Geographical distribution and seasonal variation of surface emissions and deposition velocities of atmospheric trace gases, *J. Geophys. Res.*, *97*, 3787–3804.

Olivier, J. G. J., and J. J. M. Berdowski (2001), Global emission sources and sinks, in *The Climate System*, edited by J. Berdowski, R. Guicherit, and B. Heij, pp. 33–78, Swets and Zeitlinger, Lisse, Netherlands.

Potosnak, M. J., S. C. Wofsy, A. S. Denning, T. J. Conway, J. W. Munger, and D. H. Barnes (1999), Influence of biotic exchange and combustion sources on atmospheric CO_2 concentrations in New England from observations at a forest flux tower, *J. Geophys. Res.*, *104*, 9561–9569.

Prather, M., et al. (2001), Atmospheric chemistry and greenhouse gases, in *Climate Change 2001: The Scientific Basis*, edited by J. T. Houghton et al., pp. 239–287, Cambridge Univ. Press, New York.

Roelofs, G. J., et al. (2003), Intercomparison of tropospheric ozone models: Ozone transport in a complex tropopause folding event, *J. Geophys. Res.*, *108*(D12), 8529, doi:10.1029/2003JD003462.

Sadourny, R., and K. Laval (1984), January and July performance of the LMD general circulation model, in *New Perspectives in Climate Modeling*, edited by A. Berger and C. Nicolis, pp. 173–197, Elsevier, New York.

Shindell, X., et al. (2001), Chemistry-climate interactions in the Goddard Institute for Space Studies general circulation model: 1. Tropospheric chemistry model description and evaluation, *J. Geophys. Res.*, *106*, 8047–8075.

Tiedtke, M. (1989), A comprehensive mass flux scheme for cumulus parameterization in large-scale models, *Mon. Weather Rev.*, *117*, 1779–1800.

Van Leer, B. (1977), Towards ultimate conservative difference scheme, part IV: A new approach to numerical convection, *J. Comput. Phys.*, *23*, 276–299.

Zondervan, A., and H. A. J. Meijer (1996), Isotopic characterization of CO_2 sources during regional pollution events using isotopic and radiocarbon analysis, *Tellus, Ser. B*, *48*, 601–612.

P. Bakwin, Climate Monitoring and Diagnostics Laboratory, National Oceanic and Atmospheric Administration, Boulder, CO 80305, USA.

P. Bousquet, P. Ciais, D. A. Hauglustaine, P. Peylin, and L. Rivier, Laboratoire des Sciences du Climat et de l'Environnement, CEA, Orme des Mersisiers, F-91191 Gif sur Yvette, France. (leonard.rivier@cea.fr)

A. Klonecki, NOVELTIS, Parc Technologique du Canal, 2 Av. de l'Europe, F-31520 Ramonville-Saint Agne, France.